Jan Hendrik Carstens, Clemens Gühmann

Maximum power point controller for thermoelectric generators to support a vehicle power supply

WISSEN IM ZENTRUM
UNIVERSITÄTSBIBLIOTHEK

Technische
Universität
Berlin

Maximum Power Point Controller for Thermoelectric Generators to Support a Vehicle Power Supply

Jan Hendrik Carstens[a,*], Clemens Gühmann[a]

[a]Department of Energy and Automation Technology, Chair of Electronic Measurement and Diagnostic Technology, TU Berlin, Einsteinufer 17, 10587, Berlin, Germany

Abstract

The growing mobility increases the world-wide fuel consumption. Yet the amount of fossil fuel is limited and the environmental burden is increasing dramatically as well. Many governments have enacted laws to regulate and reduce the fuel consumption as well as the CO_2 emissions of combustion engines. An idea to save fuel and to reduce the environmental burden is to use thermoelectric generators (TEGs) to recover the waste heat of the exhaust gas and convert into electric energy in automotive applications. For the linking of TEGs to the vehicle is power supply, a DC-DC converter can be used. To support a wide range of TEGs with different electric parameters, the control of DC-DC converter must be robust. Further, the control should track the maximum power point (MPP) of the TEG for an efficient power recovery. This paper presents a digital cascade controller for a boost-buck converter that charges a vehicle battery and supplies the load. To model and analyze the discontinuous converter, the state-space-averaging (SSA) is used. The tracking of the MPP is realized with a gradient algorithm and an input current control. An adaptive step size algorithm reduces the conversion time of the maximum power point tracking algorithm (MPPT). Experiments verified the controller design and the efficiency of the MPPT.

Keywords: DC-DC converter; Maximum Power Point Tracking; Thermoelectric Generator; Digital Control

Nomenclature

A_r	area
A, B	control plant polynomials
C	controller
G	control plant
R, S, T	controller polynomials
N	number of modules
P	power
S	switch
$T_{h,c}$	temperature at hot-side, cold-side
d	duty cycle
g_m	gain margin
i	current

* Corresponding author. Tel.: +49-30 314-21168; fax: +49-30 314-22120.
E-mail address: jan.h.carstens@tu-berlin.de

l	length
u	voltage
f_s	switching frequency
α_r	temperature coefficient
$\alpha, \beta, \delta, \gamma, \varepsilon$	parameters
φ_m	phase margin
ρ	Seebeck coefficient
σ	electrical conductance

1. Introduction

Today, mobility increases world-wide and is accompanied by a rising fuel consumption. This trend is in conflict with the limitation of fossil fuels. Additionally, the environmental burden is increasing dramatically. In consequence, many governments have enacted laws to reduce the CO_2 emissions of combustion engines. The resulting requirements represent a formidable challenge for research and development. Conventional internal combustion engines (ICEs) convert chemical energy, stored in fossil fuel, into mechanical energy. During this process the main part of the energy (about 50%) is dissipated as heat [1].

The recovery of the waste heat has a high potential to increase the efficiency of an ICE and consequently to reduce the fossil fuel consumption and to reduce toxic emissions. Especially the unused exhaust gas waste heat can be converted into electric power through a thermoelectric generator (TEG) [1,2]. A TEG consists of couples of n- and p-doted semiconductors. The Seebeck-effect causes a TEG to generate electrical power when a temperature gradient is applied. The maximum power of a TEG depends on the material characteristics of the semiconductors in the TEG as well as the geometric parameters of the couples [3,5]. These parameters and materials can be selected in relation to various optimization criteria.

This includes the temperature range of materials, the desired electrical rated power and the back pressure of the ICE [1,4,5,6]. This implies that TEGs must be designed and optimized for individual applications. The result is that the electrical characteristics can vary in a wide range of a TEG.

For the electrical linking of a TEG to a vehicle power supply, a DC-DC converter is necessary, if the voltage amplitudes of source and load are different. Furthermore, a DC-DC converter works in different modes. The first is the maximum power point tracking (MPPT) and the second is the trickle charging control (TCC) of the battery voltage. The MPPT is used to search and match the maximum power point of the TEG, regardless of the temperature gradient at the TEG. The result is that the alternator of the automobile needs to generate leas power. This increases the efficiency of the ICE. When the battery is charged and the power of the TEG is higher than the necessary load power, the trickle charge controller is active.
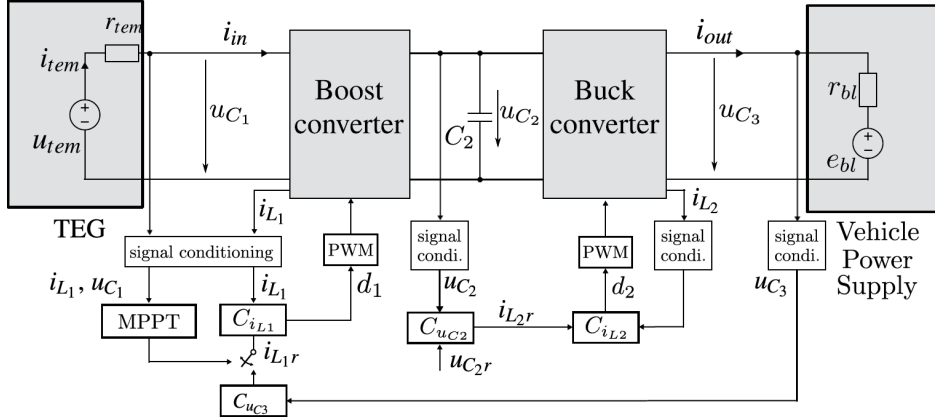
Fig. 1. Overview of control structure from boost-buck converter. The alternator is neglected the vehicle power supply.

A MPPT is based on a gradient search method and is used in particular for photovoltaic cells. This method can be applied to a TEG as well. An overview of different search algorithms is presented by Esram [7]. Beside the algorithms, the implementation of a MPPT can be divided in two general concepts: Control with and without a feedback signal [8,9,10,11].

The implementation of a feedback control loop requires a detailed system model of the converter, the load and the TEG to ensure a stable closed loop dynamic. However, a closed loop system can compensate disturbances and a desired closed loop dynamic behavior can be designed with the control parameters. In contrast to that, a MPPT without a feedback control – also called direct control – is not able to compensate feedback signals like transient oscillations which result in a higher conversion time or in a stagnation of the algorithm.

Nevertheless, the problem in designing a feedback control is the necessary knowledge of the control plants. Especially because the control plant dynamic depends on the electrical parameters of the TEG. Presented control structures [10,12] are designed based on the assumption, that the parameters of the TEG are nearly constant and well known. With this assumption the use of the converter is limited to a small number of TEGs. In contrast to that, the introduction of a robustness criterion allows to design the control parameters to compensate wide variations of the electrical parameters from a TEG.

In this paper a boost-buck converter with a feedback controller for MPPT and a control of the trickle charge voltage of the battery (see Fig. 1) is presented. The control design includes a robustness criterion to ensure a stable closed loop dynamic. The result is a regulated DC-DC converter, which is able to support a wide range of TEGs with different electrical parameters and different voltage levels of a vehicle power supply. In this context, this paper is organized as follows: The brief overview of the characteristic from a TEG is presented in section 2. In section 3 the model of the boost-buck converter is described. The digital control structure of the DC-DC converter is shown in section 4. Experimental results are presented and discussed in section 5. Finally the methods and results are summarized in section 6.

2. Thermoelectric Generator

A thermoelectric generator consists of one or more thermoelectric modules (TEMs), which are used in an application. The TEM is based on a series connection of couples of thermoelectric elements (TEs). A TE is an n- and p-doted semiconductor, with an electrical connection. Due to a temperature gradient of the TE, heat flows from the hot to the cold side. The result is that the electrons and holes of the semiconductors diffuse to the cold side and a voltage potential can be measured at the TE. This physical principle is called the Seebeck-effect, which describes the voltage Δu_{te} in relation to the temperature gradient $(T_h - T_c)$ and Seebeck coefficent ρ

$$\Delta u_{te}(T,\rho) = (\rho_p - \rho_n)(T_h - T_c) \tag{1}$$
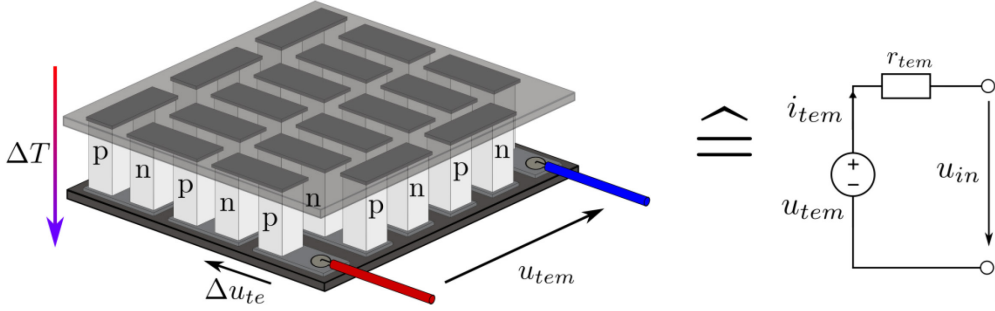
Fig. 2. TEM Module with equivalent electric circuit.

The resistor r_{te} of the couple depends on the geometry, the material parameters and the temperature

$$\Delta r_{te}(T,\sigma) = \sigma\, l\,/\, A_r (1 + \alpha_r T) \tag{2}$$

where σ is the electrical conductance, α_r is the temperature coefficient, l is the length and A_r is the area of a couple. The design parameters allow a wide variation of the electrical parameters. A detailed overview of the electrical conductance, in relation to the semiconductors is presented in Rowe [13].

Generally, the voltage of a TE is between 50 µV/K and 300 µV/K [13]. For practical use, TEs are connected in series to a TEM. The voltage u_{tem} and the resistor r_{tem} of a module yield to

$$u_{tem} = \sum_{i=1}^{N} u_{te}(i) \tag{3}$$

$$r_{tem} = \sum_{i=1}^{N} r_{te}(i) \tag{4}$$

where N is the number of the TEs in a module. With the assumption that the temperature is homogeneously distributed over a TEM and the materials are ideal, the electric equivalent circuit of a TEM can be illustrated as an ideal voltage source with an internal resistor (see Fig. 2). The relation of the electrical characteristics of a TEM to the temperature gradient is presented in Fig. 3. This example shows also the electrical power $\left(P_{tem} = u_{in} i_{tem}\right)$ curve. It can be clearly seen that only one maximum power point exists at a given temperature gradient. In this point, the output power of the TEM has the maximum.

3. Modeling of Boost-Buck converter

For the linking of the TEM to the on-board power supply, a boost-buck converter is selected. The advanteges are a high efficiency and the possibility to generate a variable output voltage [14].

The physical principle of a DC-DC converter is to charge and discharge electric storage elements like inductors or capacitors. The duration of the charging and discharging is controlled through electric switching elements, like MOSFETs. As a result, the magnitude of current and voltage of storage elements can be manipulated. The boost-buck converter includes four MOSFETs, where S_1/S_2 and S_3/S_4 are synchronized (see Fig. 4). This means, if S_1/S_3 is switched on, S_2/S_4 is off and vice versa. The MOSFETs are controlled with a pulse-width-modulation

signal (PWM) with a constant switching frequency f_s. Caused by the PWM, the converter is a non-linear time-variant system in relation to the duty cycle d. The modeling of such a system can be complex. An alternative model
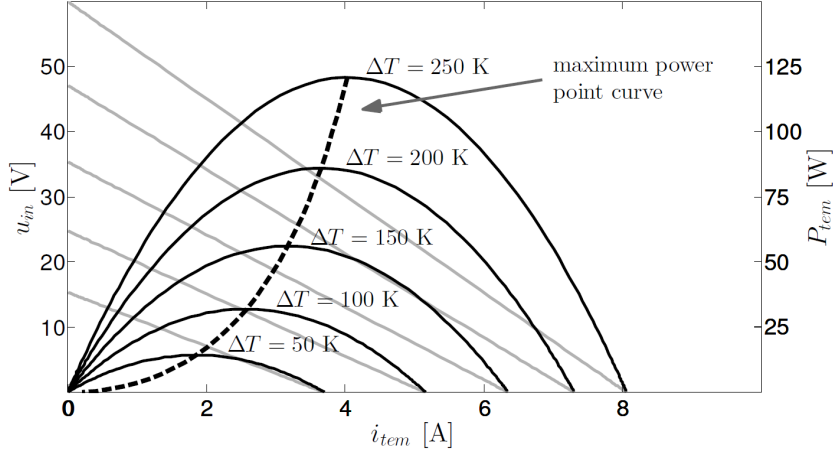
Fig. 3. Voltage and current characteristics of a simulated PbTe TEM at different temperatures (gray line) and the power curves (black line).

approach for a converter is the state-space-averaging (SSA) [15]. The idea of the SSA is to average the period changing circuit over a switching period $T_s = 1/f_s$. The result is a continuous time-invariant model. This method is accurate for frequencies up to $f_s/2$ [15]. The time derivations of voltages and currents in the boost-buck converter are:

$$\frac{du_{C_1}}{dt} = \alpha_1 u_{C_1} + \alpha_2 i_{L_1} + \alpha_3 u_{tem} \tag{5}$$

$$\frac{di_{L_1}}{dt} = \beta_1 i_{L_1} + \beta_2 u_{C_1} + \beta_3 u_{C_2} + \beta_4 u_{tem} + \beta_5 i_{L_1} d_1 + \beta_6 i_{L_2} d_2 - \beta_3 u_{C_2} d_1 - \beta_6 i_{L_2} d_1 d_2 \tag{6}$$

$$\frac{du_{C_2}}{dt} = \gamma_1 i_{L_1} + \gamma_2 i_{L_1} d_1 + \gamma_3 i_{L_2} d_2 \tag{7}$$

$$\frac{di_{L2}}{dt} = \delta_1 i_{L_2} + \delta_2 u_{C3} + \delta_3 e_{bl} + \delta_4 i_{L_2} d_2 + \delta_5 i_{L_1} d_2 + \delta_6 i_{L_1} d_1 d_2 \tag{8}$$

$$\frac{du_{C3}}{dt} = \varepsilon_1 i_{L_2} + \varepsilon_2 u_{C_3} + \varepsilon_3 e_{bl} \tag{9}$$

where d_1, d_2 are the duty cycles of S_1/S_2, S_3/S_4 and $\alpha, \beta, \gamma, \delta, \varepsilon$ are system parameters (see Appendix). The derivatives of the states $\mathbf{x} = [u_{C1}, i_{L1}, u_{C2}, i_{L2}, u_{C3}]$ are nonlinear. For the following analysis of the converter the averaged values are substituted by means of a DC and a small AC value [12]. This implies a linearization of (5) – (9) and results to the small signal state space model for the converter at the operation point

$$\dot{\mathbf{x}} = \mathbf{Ax} + \mathbf{Bu} \tag{10}$$

where **A** is the state matrix, **B** is the input matrix and $\mathbf{u} = [u_{tem}, e_{bl}, d_1, d_2]$ the input vector. All states can be measured and are filtered with a second-order low pass. The cutoff frequency is 1 kHz.
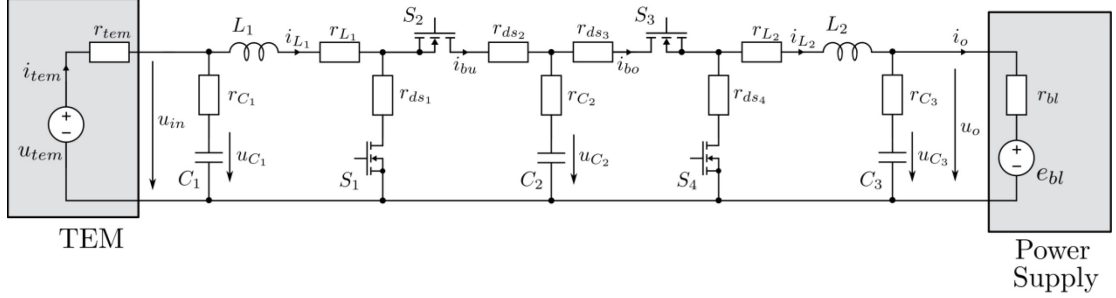
Fig. 4. Electric circuit of boost-buck converter with TEM and load.

4. Digital Control Structure

The design of the boost-buck converter is supposed to meet three requirements: The first is the maximum power point tracking (MPPT), the second is the trickle charge controller (TCC) of the load and the third is the robustness and stability of the controllers. An overview of the control structure is shown in Fig. 1. The MPPT is based on a gradient search algorithm, which uses the input current and voltage of the TEM to detect the actual power. This is realized with the boost converter. The buffer capacitor C_2 is used to decouple the two converters. A cascade controller regulates the voltage magnitude of C_2 and the output current i_{L2} to supply the load and charge the battery. In case, the output voltage u_{C3} is reaching the maximum charging voltage of the battery, the MPPT will be disabled and the trickle voltage charge controller is activated. The controllers are implemented on a microcontroller. In the next subsections the digital control structure is presented, in relation to a robustness criterion. Additionally, the MPPT algorithm and TCC are presented.

4.1. Control design

In general, the discrete time transfer function from input signal u to output signal y is defined as

$$G_{plant}(z^{-1}) = \frac{y(z^{-1})}{u(z^{-1})} = \frac{B(z^{-1})}{A(z^{-1})} \tag{11}$$

where A and B are the plant polynomials. The closed loop of a feedback control can be described by

$$G_{cl}(z^{-1}) = \frac{y(z^{-1})}{r(z^{-1})} = \frac{T(z^{-1})B(z^{-1})}{A_{cl}(z^{-1})} \tag{12}$$

where r is the reference signal, T the pre-filter polynomial of the controller and

$$A_{cl}(z^{-1}) = S(z^{-1})A(z^{-1}) + R(z^{-1})B(z^{-1}) \tag{13}$$

is the characteristic polynomial of the closed loop dynamic, in relation to the control polynomials R and S. The detailed digital control structure is shown in Fig. 5. In relation to (5) - (10) the transfer function of the boost-buck converter follow to

$$G_{d_2 u_{C2}}(z^{-1}) = \frac{u_{C_2}(z^{-1})}{d_2(z^{-1})} \tag{14}$$

$$G_{d_2 i_{L2}}(z^{-1}) = \frac{i_{L_2}(z^{-1})}{d_2(z^{-1})} \tag{15}$$

(a)

(b)

Fig. 5. Digital control loops of boost-buck converter.
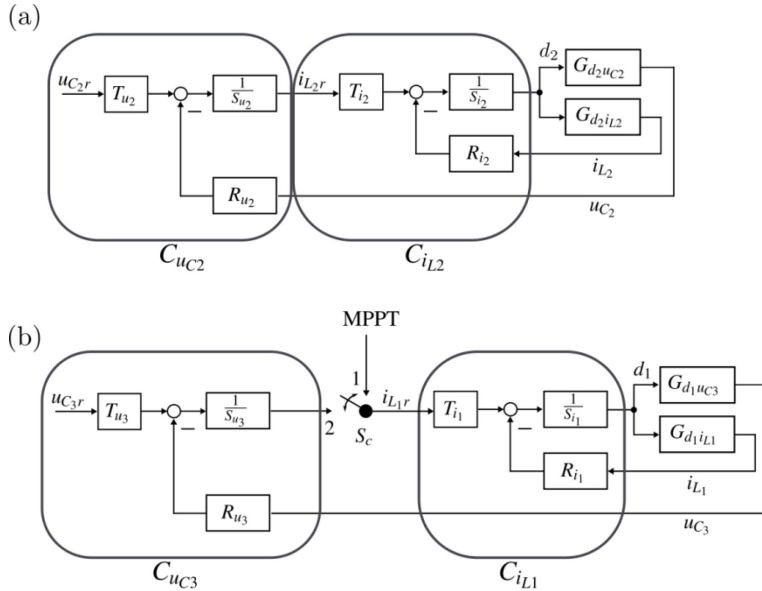
$$G_{d_1 u_{C3}}(z^{-1}) = \frac{u_{C_3}(z^{-1})}{d_1(z^{-1})} \tag{16}$$

$$G_{d_1 i_{L1}}(z^{-1}) = \frac{i_{L_1}(z^{-1})}{d_1(z^{-1})} \tag{17}$$

The control plants are sensitive to changes of the series resistance of the TEM. In Fig. 6 the frequency response of the control plant is given for different values of r_{tem}. It can be noted that the gains of $G_{d_1 u_{C3}}$ and $G_{d_2 i_{L2}}$ are significantly sensitive to r_{tem}. For small values of the resistance, the DC gain shows a maximum and decreases for higher values. However, $G_{d_2 u_{C2}}$ and $G_{d_1 i_{L1}}$ seem to be smoother, in contrast to $G_{d_1 u_{C3}}$ and $G_{d_2 i_{L2}}$ but also an influence of the parameter variation from the resistance can be detected. Hence, in all bode plots it can be seen that the control plants depend on the resistor value of the TEM. If these influences are not taken into account during the design of control parameters, the stability of the closed loop cannot be guaranteed.

In the context of the _____ f ____ ____ ___ ___ ___ ____ ____ ____ ____ ____ ___ ons gain g_m and phase margin φ_m of the ope

$$G_{ol}(z^{-1}) = \frac{B(z^{-1})K(z^{-1})}{A(z^{-1})S(z^{-1})} \tag{18}$$

can be specified [16]. A widely used approach is to define $g_m \geq 6$ dB and $\varphi_m \geq 29°$, which must satisfy all values of

r_{tem}. For this reason, the nominal resistance value of 0.1 Ω is selected, because the DC gains of $G_{d_2 i_{L2}}$ and $G_{d_1 u_{C3}}$ are maximal at this value. For higher values of the resistance, the gain and phase margin increase with a positive effect on the robustness. This characteristic is vice versa for $G_{d_1 i_{L1}}$ and $G_{d_2 u_{C2}}$, but the variation can be compensated from the controller with the selected robustness criterion. In context to this criterion, the control polynomials of the digital controller $C_{i_{L1}}$, $C_{u_{C3}}$, $C_{i_{L2}}$ and $C_{u_{C2}}$ must be designed. The control parameterization is based on a two-degree of freedom design [16]. The desired closed loop system is chosen as a second order system

$$G_{cl}(z^{-1}) \overset{!}{=} \frac{1-z^{-1}}{1} Z\left\{ \frac{G_{dcl}(s)}{s} \right\} \tag{19}$$

$$G_{dcl}(s) = \frac{\omega_o^2}{s^2 + 2D\omega_o s + \omega_o^2} \tag{20}$$

where ω_o is the natural frequency, D is the damping factor and Z is the discrete time transformation.

For the current control dynamic it is necessary to select an adequate bandwidth to compensate disturbances like load changes of the vehicle power supply and to reduce the convergence time of the desired input current of the MPPT. In contrast to that, the voltage controller can be designed with a smaller bandwidth to compensate for lower frequency control errors. The selected closed loop parameters of the controllers are presented in Table 1.

Table 1. Design parameters for controllers

Controller	ω_o [kHz]	D	Rise time [ms]
$C_{i_{L1}}$	3.14	0.95	1
$C_{i_{L2}}$	3.14	0.95	1
$C_{u_{C2}}$	0.628	0.95	5
$C_{u_{C3}}$	1.57	0.95	2.5

4.2. Maximum Power Point Tracking

In Fig. 3 the quality characteristic of a TEM and the power curves in relation to different temperature gradients are presented. In general the electric characteristics and the temperature at the TEM are unknown. The idea is to search and track the maximum power point by using a gradient algorithm. A gradient algorithm has the advantage, that not prior knowledge is necessary. In [17] a hill climbing algorithm (HC) for a boost-buck converter is presented. However, the HC algorithm uses a direct control of the MOSFETs without a feedback signal of the state signals. The problem is that signal feedbacks or disturbances can result in oscillations. In the case, that the HC recovers enough energy to charge the buffer capacitor C_2, the cascade controller increases the output current i_{L_2} and the voltage of the capacitor u_{C_2} drops down and results in a feedback signal at the signals u_{C_1} and i_{L_1}. If the HC samples the disturbance signals, the algorithm interprets this as a power change of the TEM. The algorithm reduces the duty-cycle and the input power drops down to zero. A new start of the algorithm can result in an oscillation during the start phase.

An alternative MPPT algorithm is the perturb and observe method (P&O) [7]. This algorithm uses the same gradient search method as the HC, however the P&O estimates only one new desired operation point of the input current $i_{L_1 r}$.

This desired current is the reference signal of the input current controller $C_{i_{L1}}$. In contrast to the direct control of the MOSFETs, the controller compensates disturbances of the feedback signal. The desired input current $i_{L_1 r}$ is calculated in relation to the actual input power $P_{tem}(k)$ and compared with the previous power $P_{tem}(k-1)$. If the difference $\Delta P(k) = P_{tem}(k) - P_{tem}(k-1)$ is negative, the desired input current $i_{L_1 r}$ is decreased. If $\Delta P(k) > 0$, the desired input current is increased. The MPP is reached if $\Delta P(k) = 0$. The algorithm for P&O yields to

$$i_{L_1 r}(k+1) = i_{L_1 r}(k) + \mu \, sign\left[\Delta P(k)\right] \tag{21}$$

$$sign\left[\Delta P(k)\right] := \begin{cases} +1, \Delta P > 0 \\ \ \ 0, \Delta P = 0 \\ -1, \Delta P < 0 \end{cases}$$

where μ is a constant step size. The selection of the step size influences the performance time of the P&O. For a large μ the P&O converges faster to the MPP. However, the algorithm can oscillate around the exact MPP. In contrast, the MPPT converges slower for a smaller μ, nevertheless the tracked power is closer on the MPP. An adaption of the step size combines the fast convergence time and the accuracy of a P&O:

$$\mu(k+1) = sat\left[\frac{\Delta P(k)}{\mu(k)}\right] := \begin{cases} 2\mu(k), & \dfrac{\left|\Delta P(k)\right|}{\mu(k)} > 2\mu(k) \\[3mm] \mu(k+1), & \dfrac{\mu(k)}{2} \le \dfrac{\left|\Delta P\right|(k)}{\mu(k)} \le 2\mu(k) \\[3mm] \dfrac{\mu(k)}{2}, & \dfrac{\left|\Delta P(k)\right|}{\mu(k)} < \dfrac{\mu(k)}{2} \end{cases} \tag{23}$$

The step size reduces for a small gradient of $\Delta P(k)$ and vice versa. The saturation is a boundary of the adaption size.

4.3. Trickle Charge Controller

The TCC is activated in case the load voltage reaches the maximum battery voltage u_o^+. The idea of the presented control structure (see Fig. 5) is to disable the MPPT and use the controller $C_{u_{C3}}$ to regulate the output voltage on the desired voltage $u_{C_3 r}$. For the selection of MPPT and TCC a switch S_C is used. The activation function of S_C is defined as

$$S_C := \begin{cases} 1 & , & u_o^- \ge u_{C_3} \\ 1 & 2, & u_o^- < u_{C_3} < u_o^+ \\ & 2, & u_{C_3} \ge u_o^+ \end{cases} \tag{24}$$

where u_o^- is the defined low voltage magnitude to restart the MPPT.

5. Experiments

In section 3 and 4 the modeling and the control structure are presented. To verify the theoretical design, an experimental device is used. The TEM is simulated with a constant voltage source and a series resistor. The load is a 12.5 V 72 Ah lead acid battery. The converter is controlled by a 320F28069 microcontroller from Texas Instruments, with a sampling frequency of 10 kHz. The hardware specifications of the converter are presented in Table 2.
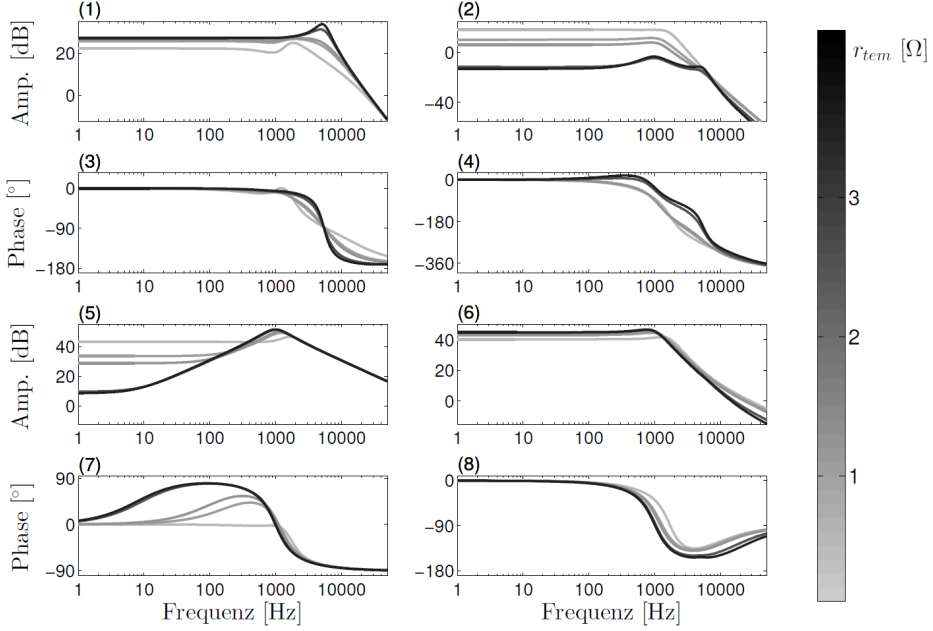
Fig. 6. Bodeplot of control plants. $G_{d_1 i_{L1}}$ is presented in (1) and (3), $G_{d_1 u_{C3}}$ is presented in (2) and (4), $G_{d_2 i_{L2}}$ is presented in (5) and (7) and $G_{d_2 u_{C2}}$ is presented in (6) and (8).

5.1. Verification of Control Design

In relation to the control requirements from Table 1 and the parameters of the converter from Table 2, the controllers $C_{i_{L1}}$, $C_{i_{L2}}$, $C_{u_{C2}}$ and $C_{u_{C3}}$ are designed for a nominal value of $u_{tem} = 30$ V and $r_{tem} = 0.1\,\Omega$. To verify the feedback controllers, the step response of each closed loop is measured (see Fig. 7). Each measured output signal of the control loop matches the desired dynamic of the control design. The deviations of the measurements are caused by noise and quantization effects of the microcontroller.

Table 2. Parameter of converter

L_1	45 μH	r_{L1}	43.2 mΩ	L_2	22.4 μH	r_{L2}	17.7 mΩ
C_1	20 μF	r_{C1}	1.2 mΩ	C_2	88 μF	r_{C2}	17.1 mΩ
C_3	30 μF	r_{C3}	0.8 mΩ	e_{bl}	12.5 V	r_{bl}	100 mΩ
S_1, S_2, S_3, S_4 Infineon IPP80N06S2L-07 , $f_s = 100$ kHz							
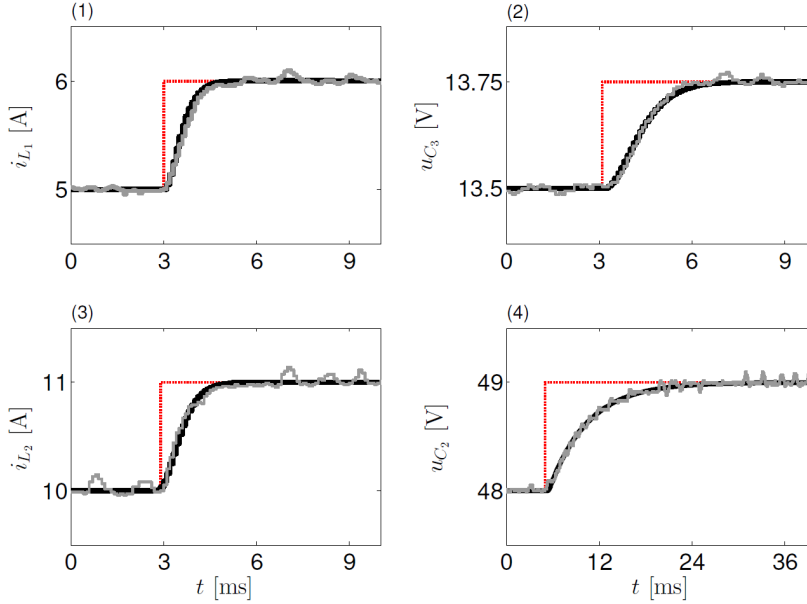
Fig. 7. Step responses of the control loops. The red dashed line is the reference signal. The black line is the desired output signal and grey the measurement. (1) shows the controlled signal of i_{L_1}, (2) the signal of u_{C_3}, (3) the signal of i_{L_2} and (4) u_{C_2}.

5.2. Verification of Maximum Power Point Tracking

In this experiment, the TEM is simulated with nominal values $u_{tem} = 15$ V and $r_{tem} = 3.1\,\Omega$ at the beginning. To verify the convergence and adaption, the resistor and the voltage are changed.

In Fig. 8 the signals of the converter and the simulated TEM are shown. After 1.5 s the MPPT is enabled and the algorithm starts to calculate the desired reference input current, which is regulated with the input current controller $C_{i_{L1}}$. After approximately 1 s the MPP is reached and the algorithm has converged. This can also directly be recognized from the measurement, because $u_{in} = 1/2\, u_{tem}$ in this case. At 3.7 s the resistor changes to 1.8 Ω. The reaction of the MPPT has a dead time of nearly 300 ms before an adaption of the new MPP can be observed. The
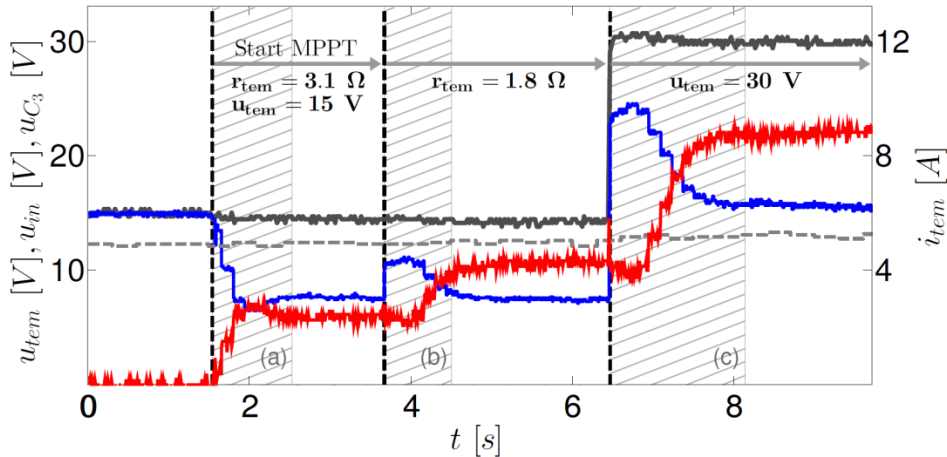
dead time is the result of the adaptive P&O algorithm (23), because the step size is reduced in relation to the previously small power difference ΔP. After the detection of the power change, the step size must increase. This dead time can also be observed when the input changes to $u_{tem} = 30\,\text{V}$.
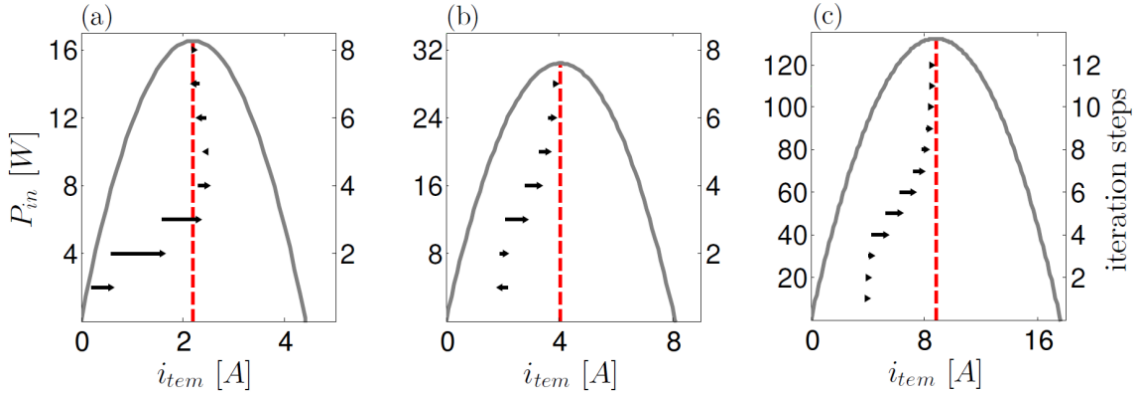
Fig. 8. Verification of MPPT algorithm. The grey line is u_{tem}, the blue line is u_{in}, the grey dashed line is the output voltage u_{C_3} and the red line is the input current i_{tem}.

disturbance is compensated by the input controller. Without the control, it would lead to an undesired increase of the current signal. Finally, the estimated gradient of the input power could be incorrect.

Nevertheless, the P&O algorithm converges in all three cases to the MPP with a maximum converge time of 2 s. Fig. 9 shows the detailed calculation and adaption of the desired input current $i_{L_1 r}$ of the MPPT algorithm for the time spans (a), (b) and (c) from Fig. 8 in relation to the actual power curves of the TEM.

5.3. Verification of Trickle Charge Controller

In this experiment, the battery was charged to 13.3 V. At the beginning of the experiment $u_{\ }= -15\,\text{V}$ and

$r_{tem} =$ Fig. 9. Step size adaption of MPPT algorithm for the time spans (a), (b) and (c) from Fig. 8.   at 40

ms an   up to

the selected maximum battery voltage $u_o^+ = 13.6$ V. At this time, the TCC is activated and the desired voltage $u_{C_3 r} = 13.4$ V is regulated. To match this voltage, the input current is reduced to 2.1 A. At 500 ms the resistor changes to $r_{tem} = 3.1\,\Omega$ and the input power is not sufficient to hold on the trickle voltage. As a consequence, the output voltage decreases and the TCC increases the input current to match the desired battery voltage. At the point that the output voltage drops down to $u_o^- = 13.3$ V, the MPPT is reactivated.
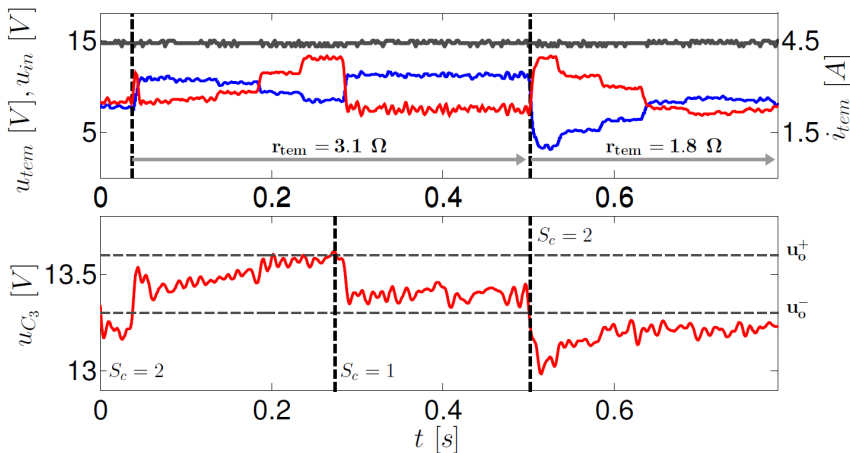
Fig. 10. Verification of TCC algorithm. The grey line is u_{tem}, the blue line is u_{in} and the red line is the input current i_{tem} at the top

6. Conclusions

In this paper a control concept for a boost-buck converter is presented. A variation of the electrical characteristics of the TEGs is analysed in the frequency domain. The series resistance of the TEG influences the state dynamic of the control plants. The operation point for the state space model is selected for the resistor value, which caused the highest DC gain of the plants. Based on this selected operation point, the linear digital controllers are designed. A robustness criterion is defined to ensure the stability of the closed loop dynamic for a variation of the electrical parameters of the TEG.

The presented MPPT is based on a perturbe and observation algorithm, which determines a desired input current. In contrast to a direct control algorithm, an oscillation at the start phase of the algorithm or disturbances can be compensated. The perturbed and observation algorithm is extended with a variable step size to reduce the oscillation at the MPP and to adapt the step size in relation to the power gradient of the actual power from the TEG. An overvoltage protection for the battery is realized with a trickle charging control. In this case, the MPPT algorithm is disabled and the desired trickle charge voltage is controlled with a cascade voltage controller. The control and algorithms are proven in experiments.

The next steps are to analyse and optimize the electrical wiring of explicit TEMs for a DC-DC converter to optimize the power efficiency. Furthermore a TEG prototype with DC-DC converter should be integrated and verified at an exhaust gas system of internal combustion engine.

Acknowledgements

Appendix

$$\alpha_1 = \frac{\alpha_2}{r_{tem}} = -\alpha_3 = -\frac{1}{C_1(r_{C_1} + r_{tem})} \tag{25}$$

$$\beta_1 = \frac{(r_{tem} + r_{C_1})\, r_{L_1} + (r_{C_1} + r_{tem})\, r_{C_2} + (r_{ds_2} + r_{tem})\, r_{C_1} + r_{ds_2} r_{tem}}{L_1(r_{tem} + r_{C_1})} \tag{26}$$

$$\beta_2 = \frac{r_{tem}}{L_1(r_{tem} + r_{C_1})} \tag{27}$$

$$\beta_3 = -\frac{\beta_6}{r_{C_1}} = -\frac{1}{L_1} \tag{28}$$

$$\beta_4 = \frac{r_{C_1}}{L_1(r_{tem} + r_{C_1})} \tag{29}$$

$$\beta_5 = \frac{r_{C_2} + (r_{ds_2} - r_{ds_1})}{L_1} \tag{30}$$

$$\gamma_1 = -\gamma_2 = -\gamma_3 = \frac{1}{C_2} \tag{31}$$

$$\delta_1 = -\frac{r_{C_3} r_{L_2} + r_{bl} r_{L_2} + r_{C_3} r_{bl} + r_{ds_3} r_{C_3} + r_{ds_3} r_{bl}}{L_2(r_{C_3} + r_{bl})} \tag{32}$$

$$\delta_2 = -\delta_3 = -\frac{r_{bl}}{L_2(r_{C_3} + r_{bl})} \tag{33}$$

$$\delta_4 = -\frac{r_{C_2} + r_{ds_4} - r_{ds_3}}{L_2} \tag{34}$$

$$\delta_5 = -\delta_6 = \frac{r_{C_2}}{L_2} \tag{35}$$

$$\varepsilon_2 = -\frac{\varepsilon_1}{r_{bl}} = -\varepsilon_3 = -\frac{1}{C_3(r_{C_3} + r_{bl})} \tag{36}$$

References

[1] R. Kühn, O. Koeppen and J. Kitte, Influence of an Optimized Thermoelectric Generator on the Back Pressure of the Subsequent Exhaust Gas System of a Vehicle, Journal of Electronic Materials, vol. 43, no. 6, 2014, pp. 1–6.

[2] J. Kitte, R. Kühn, H.-F. Pernau, K. Littmann and D. Jänsch, Dimensioning and Evaluating a Multi-Channel Thermoelectric Generator Using a Costumized Simulation Architecture, Themoelectric Goes Automotive II, 2013, pp. 207–224.

[3] H. J. Goldsmid and G. S. Nolas, A review of the new thermoelectric materials, XX International Conference on Thermoelectrics, 2001, pp. 1–6.

[4] Y. Mu, G. Chen, R. Yu, G. Li, P. Zhai and P. Li, Effect of geometric dimensions on thermoelectric and mechanical performance for Mg2Si-based thermoelectric unicouple, Materials Science in Semiconductor Processing, vol. 17, Jan 2014, pp. 21–26.

[5] D. Ebling, K. Bartholomé, M. Bartel, M. Jägle, Module geometry and contact resistance of thermoelectric generators analyzed by multiphysics simulation, Journal of electronic materials, vol. 39, no. 9, 2010, pp. 1376–1380.

[6] W. Glatz, S. Muntwyler and C. Hierold, Optimization and fabrication of thick flexible polymer based micro thermoelectric generator, Sensors and Actuators A: Physical, vol. 132, no. 1, 2006, 337–345.

[7] T. Esram and P. L. Chapman, Comparison of photovoltaic array maximum power point tracking techniques, IEEE Transactions on Energy Conversion, vol. 22, no. 2, June 2007, pp. 439–449.

[8] M. A. G de Brito, L. Galotto, L. P. Sampaio, G. de Azevedo e Melo and C. A. Canesin, Evaluation of the main MPPT techniques for photovoltaic applications, Industrial Electronics, IEEE Transactions on, vol. 60, no. 3, 2013, pp. 1156–1167.

[9] L. X. Ni, K. Sun, L. Zhang, Y. Xing, M. Chen and L. Rosendahl, A power conditioning system for thermoelectric generator based on interleaved Boost converter with MPPT control, Electrical Machines and Systems (ICEMS), 2011 International Conference on, IEEE, 2011, pp. 1–6.

[10] K. Rae-Young, L. Jih-Shen, B. York and A. Koran, Analysis and Design of Maximum Power Point Tracking Scheme for Thermoelectric Battery Energy Storage System, IEEE Transactions on Industrial Electronics, IEEE, vol. 56, no. 9, 2009, pp. 3709 –3716.

[11] J. Eakburanawat, I. Boonyaroonate, Development of a thermoelectric battery-charger with microcontroller-based maximum power point tracking technique, Journal of Applied Energy, vol. 83, no. 7, Elsevier, 2006, pp. 687–704.

[12] S. Cho, N. Kim, S. Park and S. Kim, A coreless maximum power point tracking circuit of thermoelectric generators for battery charging systems, IEEE Asian Solid-State Circuits Conference, 2010, pp. 1–4.

[13] D. M.l Rowe et. al., Thermoelectrics and its Energy Harvesting, 2-Volume Set: Modules, Systems, and Applications in Thermoelectrics, CRC Press, Boca Raton, FL, 2012.

[14] J. H. Carstens and C. Gühmann, Simulative analysis and evaluation of dc/dc converters for thermoelectric generators, 5th IAV Conference: Simulation and Testing for Automotive Electronics, 2012, pp. 145–155.

[15] R. W. Erickson, D. Maksimovic, Fundamentals of Power Electronics, second ed. Kluwer Academic Publishers, New York, 2001.

[16] I. D. Landau, G. Zito, Digital Control Systems: Design, Identification and Implementation, Springer Verlag, London, 2006.

[17] J. H. Carstens and C. Gühmann, Control concept for the electrical integration of thermoelectric generators into a vehicle power supply, 14th Internationales Stuttgarter Symposium, 2014, pp. 627–642.